HHS Public Access

Author manuscript

Magn Reson Med. Author manuscript; available in PMC 2016 June 01.

Published in final edited form as:

Magn Reson Med. 2015 June ; 73(6): 2122–2128. doi:10.1002/mrm.25336.

Comparison of MRI Methods for Measuring Whole-Brain Venous Oxygen Saturation

Suliman Barhoum, **Zachary B. Rodgers**, **Michael Langham**, **Jeremy F. Magland**, **Cheng Li**, and **Felix W. Wehrli***

Department of Radiology, University of Pennsylvania, Philadelphia, Pennsylvania, USA

Abstract

Purpose—In this work, we compare susceptometry-based oximetry (SBO) and two T_2-based methods for estimating resting baseline SvO_2 in the superior sagittal sinus (SSS).

Methods—SBO is a field-mapping technique whereas in T_2-based methods the intravascular blood signal is isolated either with velocity-encoded projections [projection-based T_2 (PT_2)] or a tag-control scheme [T_2-relaxation under spin tagging (TRUST)] after T_2-preparation. The measurements were performed on twelve healthy subjects (mean age=33±6 years) at 3 Tesla field strength. The reliability, precision, and reproducibility were examined for the three techniques.

Results—The mean (± standard deviation) SvO_2 quantified by SBO, PT_2, and TRUST were found to be 65.9±3.3, 65.6±3.5, and 63.2±4.1%. The standard deviation (SD) for 10 consecutive measurements in the quantified SvO_2 was less than 2.7%, 4.7%, and 5.0% for SBO, PT_2, and TRUST across all subjects. In testing reproducibility across different days, the resulting SDs were 2.6, 3.5, and 2.0% for SBO, PT_2, and TRUST.

Conclusion—The results indicate that all three SvO_2 quantification techniques to be reliable with good agreement between PT_2 and SBO while TRUST yielded slightly lower values compared with the other two techniques.

Keywords

SvO_2 quantification; brain oximetry; blood T_2 quantification; susceptometry-based oximetry; T_2-relaxation-under-spin tagging

INTRODUCTION

Measuring global cerebral venous oxygenation (SvO_2) in the sagittal sinus or jugular vein provides direct assessment of the brain's ability to extract and metabolize oxygen. Clinical estimation of brain oxygen saturation has traditionally been performed by jugular vein catheterization (1–3), which has risks, including venous infection and thrombosis (4). Near-infrared spectroscopy (NIRS) is a noninvasive technique that is being used both clinically and in the research setting to quantify regional oxygenation in brain tissue (5). However, NIRS quantifies superficial regional instead of global oxygenation and cannot differentiate

*Correspondence to: Felix W. Wehrli, Ph.D., Laboratory for Structural NMR Imaging, Department of Radiology, University of Pennsylvania, 1 Founders Pavilion, 3400 Spruce Street, Philadelphia, PA 19104. wehrli@mail.med.upenn.edu.

the signal of the arterial and venous blood (6). Some noninvasive MRI approaches have emerged recently for quantifying SvO_2 by means of measurement of blood T_2, such as the TRUST method (7,8) and projection-based T_2 quantification (PT_2) (9), building on earlier work by Wright et al (10).

T_2-based methods quantify the transverse relaxation of water protons in whole blood caused by spin sampling of two frequency-shifted compartments, intra- and inter-erythrocyte. Such a frequency shift is created due to local field inhomogeneity in the immediate vicinity of paramagnetic deoxyhemoglobin. Thus, a greater fraction of deoxyhemoglobin leads to enhanced signal attenuation by T_2 relaxation. However, converting the measured T_2 to SvO_2 requires an ex vivo calibration curve (11,12).

An alternative approach makes use of the induced magnetic field of intravascular blood such as in susceptometry-based oximetry (SBO) (13,14). In SBO, the vessel is modeled as a long paramagnetic cylinder (14) immersed in an external uniform magnetic field, and SvO_2 is computed based on the induced field shift in intravascular blood relative to the surrounding tissue, which serves as a calibration-free reference.

Previous studies demonstrated the utility of SBO for quantifying SvO_2 in the internal jugular (14), superior sagittal sinus (SSS) (15), and femoral veins (16). In agreement with the theoretical model, both computer simulations (17) and experimental results (15) confirmed that the method is robust to deviations from vessel circularity [such as the more triangular cross section of the SSS] for vessels with tilt angles less than 30° relative to the static magnetic field.

Detection of changes in SvO_2 in response to various physiologic stimuli has been demonstrated for both types of methods (9,18–20). For example, PT_2, SBO, and TRUST were used to detect the effect of hypercapnia on SSS SvO_2 (9,18,21). SBO was also used to detect changes in SSS SvO_2 in response to apneic challenge (19). In addition, TRUST was used to examine and quantify changes in SSS SvO_2 in response to hypoxia and hyperoxia (20).

Although data in the literature suggest agreement among the three techniques in terms of the measured SvO_2 values, these methods have never been compared under controlled conditions in the same subjects. In order for these methods to be used clinically, their reliability and mutual agreement needs to be evaluated. The purpose of this study was to perform a systematic comparison of three methods for quantifying resting baseline SvO_2 in the SSS with pulse sequences and analysis algorithms replicated to closely match those in the parent literature.

METHODS

Theory of MRI-Based SvO_2 Quantification

T_2-Based Methods—The dependence of blood T_2 on SvO_2 results from the paramagnetism of deoxygenated hemoglobin, which creates field gradients in the vicinity of red blood cells. The enhanced transverse relaxation rate R_2 can be described in terms of the

Luz-Meiboom chemical exchange model (22), which attributes this effect to irreversible dephasing of spins undergoing exchange between two compartments of different water proton resonance frequencies. The relaxation rate (R_2) in response to the Carr-Purcell-Meiboom-Gill (CPMG) pulse train can be written as (10):

$$R_2 = R_{2,0} + Hct(1-Hct)(\alpha\omega_o(1-SvO_2))^2 \times \tau \left[1 - \frac{2\tau}{\tau_{cp}} \tanh\left(\frac{\tau_{cp}}{2\tau}\right)\right] \quad [1]$$

where Hct is the hematocrit (volume fraction of erythrocytes in whole blood), τ is the exchange time of protons between the two chemically shifted sites, ω_o is the proton Larmor frequency, α is a dimensionless quantity related to the geometry of erythrocyte and the magnetic susceptibility of deoxyhemoglobin, τ_{cp} is the interecho spacing in the T_2-preparation CPMG train, and $R_{2,0}$ is the relaxation rate of fully oxygenated blood (i.e., arterial blood not in the presence of hypoxia).

Both T_2-based methods examined here use the same T_2-preparation by means of CPMG pulse trains of variable duration to confer T_2-weighting, except that the blood water signal is isolated in different ways. In TRUST, the signal is mapped and partial volume effects minimized by performing pairwise subtraction between the control and label images (7) analogous to arterial spin labeling (ASL):

$$\Delta S = S_{blood} - S_o \exp\left(eTE\left(\frac{1}{T_1} - \frac{1}{T_2}\right)\right) \quad [2]$$

where eTE is the duration of T_2-preparation portion of the sequence. T_1 is taken to be 1624 ms in keeping with previous work (7,23).

In the PT_2 method (9), the blood signal for each T_2-preparation is isolated by taking the complex difference (CD) between a pair of projections with equal and opposite velocity-encoding. Here the CD can be defined as (9):

$$|CD| = 2M \left|\sin\left(\frac{\pi V}{2VENG}\right)\right| \exp\left(-\frac{eTE}{T_2}\right) \quad [3]$$

where M depends on pulse sequence parameters (TE, TR, flip angle, and venous blood water spin density) (24), and V represents the blood flow velocity averaged over the SSS lumen. VENC should be equal to the blood flow velocity averaged over the cardiac cycle to minimize the complex difference $|CD|$ dependence on blood flow velocity (9).

Susceptometry-Based Oximetry (SBO)—Susceptometry-based oximetry relies on measurement of the magnetic susceptibility difference $\Delta\chi = \Delta\chi_{do}$ Hct ($1-SvO_2$) between the intravascular blood and surrounding tissue (13,14), where $\Delta\chi_{do} = 4\pi$ (0.27) ppm (25) is the susceptibility difference (in SI units) between fully deoxygenated and fully oxygenated blood. Thus, $\Delta\chi_{do}$ is a universal constant that is independent of sequence parameters and the subject's hematocrit level. If the vessel is modeled as a long cylinder of length much greater than the diameter, the induced magnetic field (ΔB) relative to the surrounding tissue can be approximated as (14):

$$\Delta B \approx \frac{1}{6}\Delta\chi B_o(3\cos^2\theta - 1) = \frac{1}{6}\Delta\chi_{\mathrm{do}} Hct(1 - SvO_2)B_o(3\cos^2\theta - 1) \quad [4]$$

where θ is the vessel tilt angle relative to the main field (B_o).

Pulse Sequences for *SvO_2* Quantification

TRUST—The pulse sequence used was analogous to that described by Xu et al (26). It consists of a nonselective T_2-preparation CPMG pulse train (10,27) (τ_{cp}=10 ms) composed of 180° composite pulses to impart T_2-weighting. The duration of the CPMG train is defined in terms of an effective echo time (eTE). For each eTE, a single-shot echo planar imaging (EPI) readout was used to scan k-space twice, both with and without tagging of venous blood superior to the imaging slice. Scan parameters are: imaging slice thickness=10 mm, labeling slab thickness=50 mm, gap between imaging slice and labeling slab=25 mm, field of view (FOV)=230 × 230 mm^2, matrix size=64 × 64 with 5/8 partial Fourier sampling, repetition time (TR)=3000 ms, EPI echo time=7.47 ms, and inversion time (TI) between blood tagging and imaging =1200 ms, yielding a temporal resolution of 24 s. T_2 was computed by fitting the amplitudes obtained at eTEs=0, 40, 80, and 160 ms to an exponential decay and T_2 was converted to *SvO_2* based on the calibration curve given in (12).

PT_2—The pulse sequence used has been described by Jain et al (9). The sequence includes a nonselective T_2-preparation CPMG train (τ_{cp}=10 ms) similar to that used in TRUST. However, only the two central k-space lines with opposite velocity encodings (±VENC) were acquired for each eTE. In distinction to the TRUST sequence, eTE values were corrected for analysis to account for the periods the magnetization is longitudinal as a result of the composite 180° pulses (28). Hence, in lieu of 20, 40, 80, and 160 ms, values of 18.3, 36.6, 73.2, and 146.5 ms were used to compute T_2, matching the values reported for the derivation of the calibration curve (11). Scan parameters are: imaging slice thickness=5 mm, FOV=176 × 176 mm^2, matrix size=176 × 1, TR=1875 ms, and TE=10.2 ms, yielding a temporal resolution of 15 seconds. Note that the faster temporal resolution relative to TRUST is achieved by use of complex difference processing to isolate the blood signal, eliminating the need to wait over a second (TI=1200 ms) for blood to flow from the tagging slab to the imaging slice. The shorter projection readout TR (compared with that of the EPI readout used in TRUST) also improves temporal resolution slightly. VENC was set to 20 cm/s, close to the average blood flow velocity in the SSS to minimize sensitivity of T_2 to SSS venous blood variation (9).

SBO—The pulse sequence was designed to simultaneously quantify *SvO_2* in the SSS and average blood flow velocity in internal carotid and vertebral arteries (15). It is composed of four interleaves that are repeated to collect two flow-compensated gradient echoes differing in TE (interleaves 1 and 3) at the level of the SSS, and a pair of gradient echoes (interleaves 2 and 4) at the same TE, but differing in first gradient moment (0 and ≠0), at the level of the neck. Scan parameters are: imaging slice thickness=5 mm, field of view (FOV)=208 × 208 mm^2, matrix size=208 × 208, flip angle=25°, TR=35 ms (effective TR at each slice=70 ms),

VENC=60 cm/s, and ΔTE=7.04 ms for interleaves 1 and 3, yielding a temporal resolution of 30 s.

MR Imaging Experiments

All imaging was performed at 3 Tesla (T) on a Siemens Tim Trio system with a 12-channel head and neck coil combination. Twelve healthy human subjects (mean age=33±6 years, 3 females and 9 males) participated in the study, which was approved by the Institutional Review Board (IRB) of the University of Pennsylvania. Resting baseline measurements were performed with each of the three techniques in each subject at the level of the SSS. Each examination included 10 successive measurements for each technique, for a total scan time of 11 min. All pulse sequences were programmed using SequenceTree (29). The execution order of the three sequences was permuted among subjects to minimize bias. After completion of the MRI exams, the Hct level was measured for each subject by means of capillary blood sample obtained from the fingertip (Hb 201+, Hemocue, Angelholm, Sweden).

Intrasubject reproducibility measurements were conducted in four healthy males (mean age 35±8 years). Each subject was scanned in three separate sessions, at least one day apart but all within a 2-week period, following the same MRI protocol.

Image Processing and Analysis

TRUST—Difference images were obtained at eTEs of 0, 40, 80, and 160 ms and a region of interest encompassing the SSS with four voxels containing the largest difference signal manually selected from the eTE=0 ms image. The data were then fitted to Eq. [2] to calculate T_2 using unadjusted eTEs (i.e., without accounting for the duration of the 180° composite pulses in the T_2-preparation CPMG train). This is necessary as the calibration equation used for converting T_2 values to SvO_2 (12):

$$R_2=\frac{1}{T_2}=A+B(1-SvO_2)+C(1-SvO_2)^2 \quad [5]$$

was derived using T_2 values calculated with unadjusted eTE values. In Eq. [5], A, B, and C are constants (listed in Table 1) depending on the Hct for each subject and the τ_{cp} (10 ms in this study).

PT_2—T_2-weighted projection images were obtained at eTEs of 20, 40, 80, and 160 ms. A region of interest including the four voxels containing the largest difference signal was drawn manually from the eTE=20 ms image. CD images were then fitted to Eq. [3] using eTEs adjusted for the time of the 180° composite pulses (18.3, 36.6, 73.2, and 146.5 ms) (28) to quantify T_2. T_2 values were converted to SvO_2 using an ex vivo calibration curve derived with the adjusted eTE values (11):

$$R_2=\frac{1}{T_2}=\frac{1}{T_{2,o}}+K(1-SvO_2)^2 \quad [6]$$

The constant K is a function of α, ω_o, Hct and ($\tau_{cp}/2\tau$) in Eq. [1]. This calibration curve was determined for four Hct levels within the physiologic range. SvO_2 values were interpolated from the calibration curve to match each subject's Hct.

SBO—A phase difference image was computed from echoes 1 and 3 as $\Delta\phi_{map}=\arg(Z_1 Z_3^*)=\gamma\Delta B\Delta TE$, where Z_1 and Z_3 are the complex pixel values of the two echoes and the asterisk indicates the complex conjugate. To reduce the effects of static background field inhomogeneity in the constructed phase image resulting from air–tissue interfaces, a retrospective correction method was implemented by fitting the static field inhomogeneity to a second-order polynomial (30). Subsequently, the phase difference (Δφ) between intravascular blood and surrounding tissue was used to quantify SvO_2 as:

$$SvO_2=\left[1-\frac{2|\Delta\phi|}{\gamma\chi_{do}\Delta TEB_o(\cos^2\theta-1/3)Hct}\right] \quad [7]$$

Hct was determined from a capillary blood sample for each subject. The tilt angle (θ) of the vessel with respect to the main magnetic field was measured from the scout images.

The superior sagittal sinus ROI was selected based on thresholding of complex difference images, which robustly isolates the vessel signal. A region of interest containing approximately 100 voxels of white and gray matter was drawn in the vicinity of the SSS to minimize effects of small variations in magnetic field (see Figure 1).

RESULTS

Figure 1 shows an example of (a) magnitude and (b) phase difference images obtained by SBO at the level of the SSS. Figure 2 illustrates the steps involved in calculating T_2-values by means of the PT_2 method. The localizer and projection images, the latter displayed versus eTE, are presented in Figures 2a and b, and Figure 2c shows the signal plotted versus eTE. Similarly, the steps involved to calculate T_2 by means of TRUST are presented in Figure 3. An example of cropped TRUST difference images as a function of eTE is shown in Figure 3a, and Figure 3b shows the difference signals as a function of eTE.

SvO_2 values quantified with the three techniques (SBO, PT_2, and TRUST) for the twelve study subjects are listed in Table 2. Average SvO_2 values were 65.9±3.3, 65.6±3.5, and 63.2±4.1% for SBO, PT_2, and TRUST, respectively. Two-way analysis of variance treating methods as a fixed and subjects as a random effect showed the difference between the methods to be significant ($P<0.005$). Thus, a one sample paired t-test was performed post hoc on each of the three pairs of data. PT_2 and SBO did not differ ($P=0.7$), however, TRUST-derived SvO_2 values were found to be different from those quantified with SBO ($P<0.01$) and PT_2 ($P<0.05$). Figure 4 shows correlations of the quantified SvO_2 between the different methods: PT_2 versus SBO (Fig. 4a), TRUST versus PT_2 (Fig. 4b), and TRUST versus SBO (Fig. 4c). Table 3 displays mean and SD of SvO_2 measured three times on separate days for 4 of the 12 subjects with each of the three techniques. Average SvO_2 values were 66.7±2.6, 66.1±3.5, and 64.2±2.0% for SBO, PT_2, and TRUST.

DISCUSSION AND CONCLUSIONS

Previous studies have demonstrated the robustness of SBO (15,19), PT_2 (9), and TRUST for SvO_2 quantification (7,20,21). However, these techniques have not been directly compared in a controlled manner in the same cohort of subjects. In this study, we performed a systematic comparison of these three techniques in healthy subjects at resting baseline.

Mean SSS SvO_2 for SBO, PT_2, and TRUST are in good overall agreement with those reported previously (7,9,15). For all three techniques examined in this work, vessel ROI selection was performed in a semi-automated manner, therefore greatly reducing rater dependence. For both TRUST and PT_2, we followed the same selection criteria that were used and described previously (7), selecting the four voxels containing the largest difference signals in the eTE=0 ms image (TRUST) or eTE=20 ms image (PT_2) to estimate the signal decay constant from Eqs. [2] and [3]. For SBO, a region of interest (ROI) that includes approximately 100 voxels of white and gray matter was drawn in the vicinity of the superior sagittal sinus as indicated in Figure 1. In addition, the superior sagittal sinus ROI was selected based on thresholding of complex difference images, which robustly isolates the vessel signal. This semi-automated approach makes the analysis relatively free from rater dependence.

Each measurement was repeated 10 times consecutively in each session resulting in SD in the quantified SvO_2 of less than 2.7%, 4.7%, and 5.0% for SBO, PT_2, and TRUST across all subjects (Table 2). Some of these intrasubject SvO_2 variations are likely physiologic. To test the reproducibility of the methods, the measurements were repeated in triplicate on different days in four of the subjects (Table 3) yielding SDs of 2.6, 3.5, and 2.0% for SBO, PT_2, and TRUST, respectively, suggesting excellent serial reproducibility. Because the reported values for each method in the intersession results were averaged over 10 successive measurements on each day, the data suggest short-term, i.e., intrasession, variability to be larger than longer-term, i.e., intersession, variability. This suggests that the variability due to random measurement noise (which is largely removed by averaging over the 10 repeats and thus does not contribute to the intersession variability) is greater than any true physiologic drift across different days. This indicates that resting state SvO_2 is a stable and reproducible physiologic parameter, and supports the use of averaging over multiple consecutive measurements to improve SvO_2 estimation precision.

The SvO_2 values quantified from the three techniques were highly correlated with each other (R_2=0.51, P<0.01), (R_2=0.48, P<0.05), and (R_2=0.50, P<0.05) (Figs. 4a–c). Furthermore, for each of the three correlation plots, the 95% confidence intervals for the slope of the regression line includes the line of identity. This suggests that the bias between the various methods does not have a statistically significant SvO_2 dependence over the range of SvO_2 values measured. A small discrepancy in mean SvO_2 measured with the two T_2-based methods was observed. TRUST yielded an average SvO_2 value lower by 2.4% relative to PT_2 which was statistically significant (P=0.019). One potential source of this discrepancy may be the longer echo time used in the EPI readout of our TRUST sequence relative to more recent implementations by Xu et al (26). In that work, longer echo time was shown to lead to an overestimation of R_2, and thus underestimation of SvO_2, compared with a shorter

(3.6 ms) echo time achieved with parallel imaging (26). The authors of that study found a 2 s^{-1} overestimation of R_2 for a 7.0 ms versus 3.6 ms TE, corresponding to approximately 3% underestimation of SvO_2. This could explain our observed lower SvO_2 in TRUST relative to PT_2. Another potential source of the discrepancy could be differences in the readout (EPI in TRUST versus projection in PT_2) or blood isolation scheme (tag/control subtraction in TRUST versus phase contrast complex difference in PT_2) used in the two techniques. Both these factors are expected to influence signal signal to noise ratio, especially at the longer eTEs, which could create a bias in the calculated R_2. This potential effect could be further investigated by directly comparing R_2 quantified from sequences with different readouts (EPI versus projection) or blood isolation schemes (tag/control versus complex difference), but which are otherwise identical.

Another difference between the two T_2-based methods is that corrected eTEs were used for the PT_2 calibration curve used in (9), in contrast to uncorrected ones in the TRUST work by Lu and Ge (7). While substitution of signal values from one calibration curve to another results in a less than 1% difference in quantified SvO_2 values, use of the correct eTE values (T_1 corrected for PT_2, uncorrected for TRUST) is more important, as calculating SvO_2 with corrected eTE values in TRUST results in a 3% reduction in quantified SvO_2, which would have suggested a 6% underestimation of SvO_2 in TRUST relative to PT_2, erroneously suggesting a much larger discrepancy between the two T_2-based methods in our study than was actually observed. This demonstrates the fact that T_2 calibration curves are specific to a particular method and not interchangeable. The need for a sequence specific calibration curve highlights one disadvantage of T_2-based SvO_2 quantification methods in comparison to SBO, as discussed further below.

Each of the three methods has distinct advantages and disadvantages for quantification of SvO_2. SBO requires a suitable adjacent reference tissue and correction for the vessel tilt angle (θ) with respect to the external magnetic field (B_o) (14). It is also sensitive to the induced magnetic field inhomogeneity at the air–tissue interface or between adjacent tissues types (30,31). Therefore, using SBO to quantify oxygenation level in the jugular vein is challenging due to the presence of oropharynx and its proximity to the trachea, which causes severe static field inhomogeneity. In addition, vessels are modeled as long cylinders. While this approximation has been shown to cause only small errors (17), it limits the method's applicability to certain vessels such as jugular vein, femoral vein, and superior sagittal sinus (SSS).

Unlike SBO, T_2-based methods are not limited by vessel orientation, the need for a suitable reference tissue, or the vessel's proximity to sources of background field gradient such as the trachea. For example, PT_2 and TRUST have been successfully applied to SvO_2 quantification along the internal jugular vein (8,9). However, one major limitation of the T_2 methods is that a calibration curve must be separately derived for each field strength, pulse sequence, and Hct, whereas these parameters are explicitly included in the SBO model. Factors such as the freshness of the blood, different species of the blood, and experimental temperatures influence the measured T_2. For example, long-term storage of blood sample causes the formation of paramagnetic methemoglobin, which cannot bind oxygen. Additionally, variation in the erythrocyte size for blood samples from different species (e.g.

human, rodent, or bovine) causes alterations in the erythrocyte permeability (32), which influences the quantified SvO_2.

Though based on the same principle, the PT_2 and TRUST methods have specific advantages and limitations. Because the complex difference signal of flowing blood is modulated by flow velocity, PT_2 can only be applied in situations where the blood flow is relatively nonpulsatile and not changing over time. Therefore, it is not suitable to detect changes in SSS oxygenation in response to dynamic stimuli such as apnea during which flow changes occur over seconds (19). Another potential limitation of this method is that the vessel is spatially resolved in one dimension, requiring appropriate selection for the FOV to avoid vessel overlap. In contrast, TRUST uses a 2D EPI readout and therefore is not susceptible to vessel overlap as in PT_2.

SBO has the added benefit of allowing for simultaneous quantification of total cerebral blood flow with relatively high temporal resolution for quantifying $CMRO_2$. For example, in some of the authors' recent work, $CMRO_2$ was measured at 30 s temporal resolution in response to hypercapnia (15) and three seconds temporal resolution in response to apnea (19). High temporal resolution SBO has been applied outside the brain as well. A SBO sequence with 1.25 second temporal resolution SvO_2 quantification and simultaneous 120 ms temporal resolution projection-based flow quantification was implemented to evaluate the vascular response of femoral/popliteal vessels during a cuff-induced ischemia paradigm (16). Thus, SBO is well suited to study the temporal variations in SvO_2 and $CMRO_2$ in response to a variety of physiologic challenges in different organ systems.

In conclusion, we performed a systematic comparison of susceptometry-based oximetry (SBO) and two T_2-based methods (projection based T_2 (PT_2) and TRUST) for quantification SvO_2 in the superior sagittal sinus (SSS) at resting baseline. The results indicate good agreement between the SBO and PT_2 with average SvO_2 values 65.9±3.3 and 65.6±3.5, respectively, while TRUST showed a mean SvO_2 of 63.2±4.1% which is lower by less than 3% compared with SBO and PT_2. Choice of an optimal method should be based on application specific considerations, such as the availability of an appropriate calibration curve in T_2 methods, the target vessel of interest, and the desired temporal resolution.

Acknowledgments

This work was supported by NIH grants R21 HD069390, R01 HL109545, K25 HL111422, and the Howard Hughes Medical Institute International Student Research Fellowship.

References

1. White H, Baker A. Continuous jugular venous oximetry in the neurointensive care unit - a brief review. Can J Anaesth. 2002; 49:623–629. [PubMed: 12067878]
2. Jakobsen M, Enevoldsen E. Retrograde catheterization of the right internal jugular vein for serial measurements of cerebral venous oxygen content. J Cereb Blood Flow Metab. 1989; 9:717–720. [PubMed: 2777938]
3. Wilder-Smith OH, Fransen P, de Tribolet N, Tassonyi E. Jugular venous bulb oxygen saturation monitoring in arteriovenous malformation surgery. J Neurosurg Anesthesiol. 1997; 9:162–165. [PubMed: 9100188]

4. Kusminsky RE. Complications of central venous catheterization. J Am Coll Surg. 2007; 204:681–696. [PubMed: 17382229]
5. Kim MN, Durduran T, Frangos S, et al. Noninvasive measurement of cerebral blood flow and blood oxygenation using near-infrared and diffuse correlation spectroscopies in critically brain-injured adults. Neurocrit Care. 2010; 12:173–180. [PubMed: 19908166]
6. Dieters, Erik I.; SHH; Kalisvaart, Marit; Mik, Egbert G. Near Infrared Spectroscopy: an asset to the diagnosis and treatment of traumatic brain injury. Erasmus J Med. 2011:23–26.
7. Lu HZ, Ge YL. Quantitative evaluation of oxygenation in venous vessels using T2-relaxation-under-spin-tagging MRI. Magn Reson Med. 2008; 60:357–363. [PubMed: 18666116]
8. Xu F, Ge Y, Lu H. Noninvasive quantification of whole-brain cerebral metabolic rate of oxygen (CMRO2) by MRI. Magn Reson Med. 2009; 62:141–148. [PubMed: 19353674]
9. Jain V, Magland J, Langham M, Wehrli FW. High temporal resolution in vivo blood oximetry via projection-based T(2) measurement. Magn Reson Med. 2013; 70:785–790. [PubMed: 23081759]
10. Wright GA, Hu BS, Macovski A. 1991 I.I. Rabi Award. Estimating oxygen saturation of blood in vivo with MR imaging at 1. 5 T. J Magn Reson Imaging. 1991; 1:275–283. [PubMed: 1802140]
11. Qin Q, Grgac K, van Zijl PC. Determination of whole-brain oxygen extraction fractions by fast measurement of blood T(2) in the jugular vein. Magn Reson Med. 2011; 65:471–479. [PubMed: 21264936]
12. Lu HZ, Xu F, Grgac K, Liu PY, Qin Q, van Zijl P. Calibration and validation of TRUST MRI for the estimation of cerebral blood oxygenation. Magn Reson Med. 2012; 67:42–49. [PubMed: 21590721]
13. Haacke EM, Lai S, Reichenbach JR, Kuppusamy K, Hoogenraad FGC, Takeichi H, Lin WL. In vivo measurement of blood oxygen saturation using magnetic resonance imaging: a direct validation of the blood oxygen level-dependent concept in functional brain imaging. Hum Brain Mapp. 1997; 5:341–346. [PubMed: 20408238]
14. Fernandez-Seara MA, Techawiboonwong A, Detre JA, Wehrli FW. MR susceptometry for measuring global brain oxygen extraction. Magn Reson Med. 2006; 55:967–973. [PubMed: 16598726]
15. Jain V, Langham MC, Wehrli FW. MRI estimation of global brain oxygen consumption rate. J Cereb Blood Flow Metab. 2010; 30:1598–1607. [PubMed: 20407465]
16. Langham MC, Floyd TF, Mohler ER III, Magland JF, Wehrli FW. Evaluation of cuff-induced ischemia in the lower extremity by magnetic resonance oximetry. J Am Coll Cardiol. 2010; 55:598–606. [PubMed: 20152564]
17. Li C, Langham MC, Epstein CL, Magland JF, Wu J, Gee J, Wehrli FW. Accuracy of the cylinder approximation for susceptometric measurement of intravascular oxygen saturation. Magn Reson Med. 2012; 67:808–813. [PubMed: 21858859]
18. Jain V, Langham MC, Floyd TF, Jain G, Magland JF, Wehrli FW. Rapid magnetic resonance measurement of global cerebral metabolic rate of oxygen consumption in humans during rest and hypercapnia. J Cereb Blood Flow Metab. 2011; 31:1504–1512. [PubMed: 21505481]
19. Rodgers ZB, Jain V, Englund EK, Langham MC, Wehrli FW. High temporal resolution MRI quantification of global cerebral metabolic rate of oxygen consumption in response to apneic challenge. J Cereb Blood Flow Metab. 2013; 33:1514–1522. [PubMed: 23838827]
20. Xu F, Liu P, Pascual JM, Xiao G, Lu H. Effect of hypoxia and hyperoxia on cerebral blood flow, blood oxygenation, and oxidative metabolism. J Cereb Blood Flow Metab. 2012; 32:1909–1918. [PubMed: 22739621]
21. Xu F, Uh J, Brier MR, Hart J Jr, Yezhuvath US, Gu H, Yang Y, Lu H. The influence of carbon dioxide on brain activity and metabolism in conscious humans. J Cereb Blood Flow Metab. 2011; 31:58–67. [PubMed: 20842164]
22. Luz Z, Meiboom S. Nuclear magnetic resonance study of protolysis of trimethylammonium ion in aqueous solution - order of reaction with respect to solvent. J Chem Phys. 1963; 39:366–370.
23. Lu H, Clingman C, Golay X, van Zijl PC. Determining the longitudinal relaxation time (T1) of blood at 3. 0 Tesla. Magn Reson Med. 2004; 52:679–682. [PubMed: 15334591]
24. Thompson RB, McVeigh ER. Real-time volumetric flow measurements with complex-difference MRI. Magn Reson Med. 2003; 50:1248–1255. [PubMed: 14648573]

25. Spees WM, Yablonskiy DA, Oswood MC, Ackerman JJH. Water proton MR properties of human blood at 1. 5 Tesla: magnetic susceptibility, T-1, T-2, T-2* and non-Lorentzian signal behavior. Magn Reson Med. 2001; 45:533–542. [PubMed: 11283978]

26. Xu F, Uh J, Liu P, Lu H. On improving the speed and reliability of T2-relaxation-under-spin-tagging (TRUST) MRI. Magn Reson Med. 2012; 68:198–204. [PubMed: 22127845]

27. Levitt MH, Freeman R. Compensation for pulse imperfections in NMR spin-echo experiments. J Magn Reson. 1981; 43:65–80.

28. Foltz WD, Stainsby JA, Wright GA. T2 accuracy on a whole-body imager. Magn Reson Med. 1997; 38:759–768. [PubMed: 9358450]

29. Magland, F.; Wehrli, FW. Pulse sequence programming in a dynamic visual environment. Proceedings of the 14th Annual Meeting of ISMRM; Seattle, Washington, USA. p. Abstract 578

30. Langham MC, Magland JF, Floyd TF, Wehrlil FW. Retrospective correction for induced magnetic field inhomogeneity in measurements of large-vessel hemoglobin oxygen saturation by MR susceptometry. Magn Reson Med. 2009; 61:626–633. [PubMed: 19107914]

31. Wang Y, Yu Y, Li D, Bae KT, Brown JJ, Lin W, Haacke EM. Artery and vein separation using susceptibility-dependent phase in contrast-enhanced MRA. J Magn Reson Imaging. 2000; 12:661–670. [PubMed: 11050635]

32. Gardener AG, Francis ST, Prior M, Peters A, Gowland PA. Dependence of blood R2 relaxivity on CPMG echo-spacing at 2. 35 and 7 T. Magn Reson Med. 2010; 64:967–974. [PubMed: 20715058]

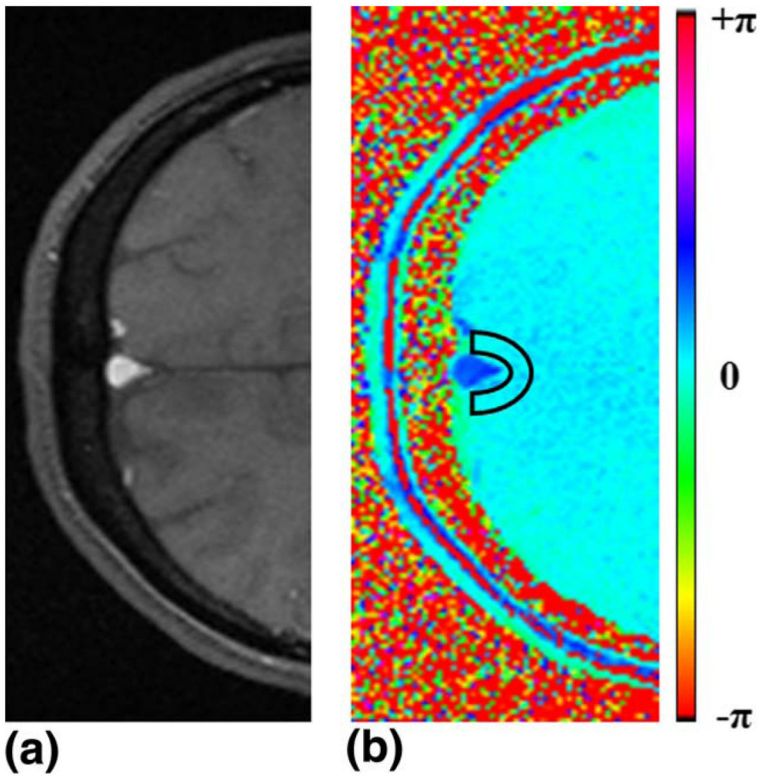

FIG. 1.

Magnitude (**a**) and phase (**b**) images at the level of SSS. The region of interest of the background tissue is denoted by the black box.

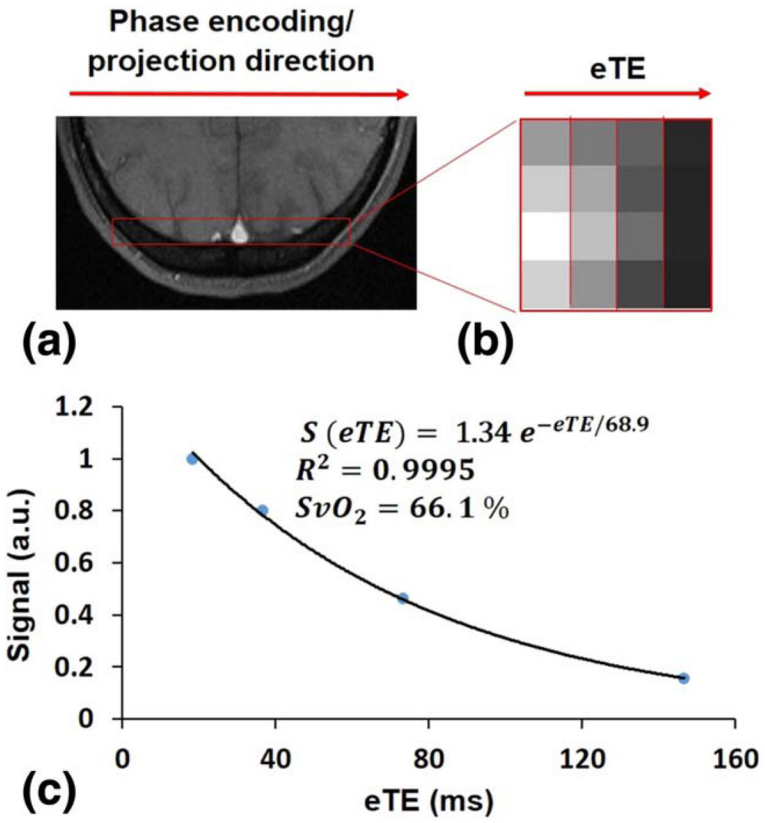

FIG. 2.

Axial magnitude image of the SSS (**a**), T2-weighted projections at eTE=18.3, 36.6, 73.2, and 146.5 ms (**b**), and signal versus eTE (**c**).

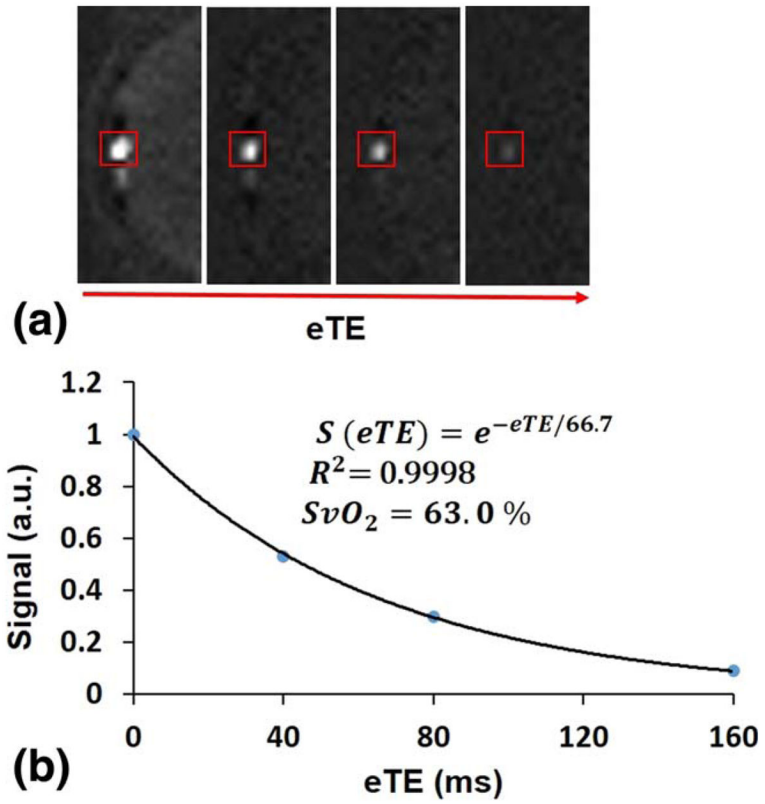

FIG. 3.

TRUST difference images at eTE=0, 40, 80, and 160 ms at the level of SSS (**a**) and signal versus eTE (**b**).

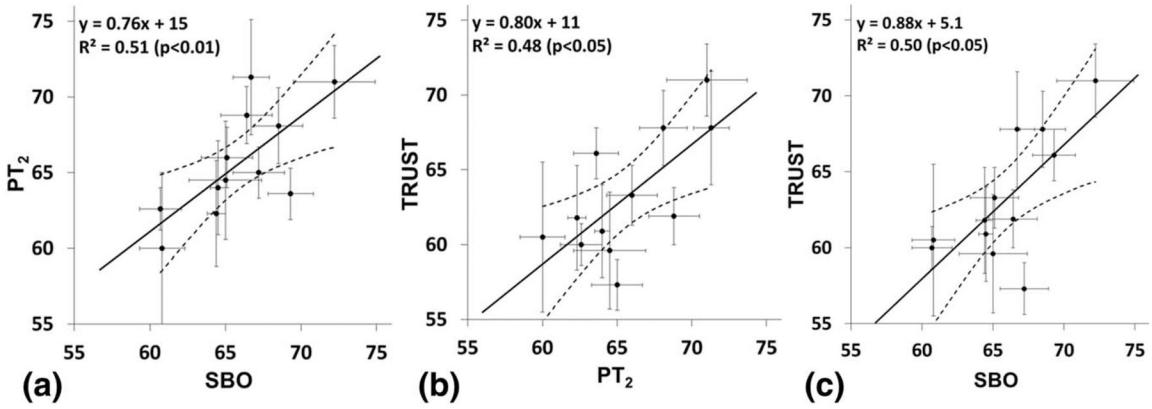

FIG. 4.

Correlations comparing measured SvO_2 (%) between PT_2 versus SBO (**a**), TRUST versus PT_2 (**b**), and TRUST versus SBO (**c**) for all 12 subjects. Error bars represent intrascan standard deviations. The dashed lines denote the 95% confidence interval for the linear fit.

Table 1

A, B, and C Parameters of TRUST Calibration Equation (i.e., Eq. [5])

Subject #	A (s^{-1})	B(s^{-1})	C(s^{-1})
1	7.094	0.438	60.96
2	7.332	0.489	61.45
3	7.289	0.479	61.37
4	5.971	0.297	58.17
5	7.067	0.433	60.90
6	7.616	0.594	61.85
7	7.382	0.503	61.55
8	7.616	0.594	61.85
9	7.321	0.487	61.43
10	5.379	0.249	56.58
11	6.982	0.419	60.71
12	5.971	0.297	58.17

Table 2

SvO_2 (%, Mean±SD) for 12 Subjects Obtained with SBO, PT_2, and TRUST

	SvO_2 (%)		
Subject #	**SBO**	**PT_2**	**TRUST**
1	72.2±2.7	71.0±4.7	71.0±2.4
2	64.5±0.5	64.0±2.4	60.9±3.1
3	60.8±1.5	60.0±3.0	60.5±5.0
4	65.0±2.4	64.5±3.4	59.6±3.9
5	64.4±0.6	62.3±1.8	61.8±3.5
6	66.4±1.7	68.8±2.7	61.9±1.9
7	66.7±1.2	71.3±4.3	67.8±3.8
8	68.5±1.6	68.1±1.7	67.8±2.5
9	69.3±1.5	63.6±2.1	66.1±1.7
10	60.7±1.4	62.6±2.7	60.0±1.4
11	65.1±1.7	66.0±2.0	63.3±2.0
12	67.2±1.7	65.0±4.0	57.3±1.7
Mean±SD	65.9±3.3	65.6±3.5	63.2±4.1

Table 3

Summary of Intersession SvO_2 (%, Mean±SD) in Four Subjects[a]

	SvO_2 (%)		
Subject #	**SBO**	**PT_2**	**TRUST**
1	64.7±1.5	65.0±1.0	62.7±2.1
2	64.3±1.5	63.7±1.5	62.3±0.6
3	68.3±2.1	71.3±4.0	65.3±5.8
4	69.5±0.7	64.5±0.7	66.5±0.7
Mean±SD	66.7±2.6	66.1±3.5	64.2±2.0

[a]Means are from three repeated measures on separate days for SBO, PT_2, and TRUST.